

Article

Design, Synthesis and Biological Assessment of *N'*-(2-Oxindolin-3-ylidene)-6-methylimidazo[2,1-*b*]thiazole-5-carbohydrazides as Potential Anti-Proliferative Agents toward MCF-7 Breast Cancer

Najla A. Alshaye¹, Mohamed K. Elgohary^{2,*}, Mahmoud S. Elkotamy²  and Hatem A. Abdel-Aziz^{3,*}

¹ Department of Chemistry, College of Science, Princess Nourah bint Abdulrahman University, P.O. Box 84428, Riyadh 11671, Saudi Arabia; naalshaye@pnu.edu.sa

² Pharmaceutical Chemistry Department, Faculty of Pharmacy, Egyptian-Russian University, Cairo 11829, Egypt; mahmoud-elkotamy@eru.edu.eg

³ Applied Organic Chemistry Department, National Research Center, Dokki, Cairo 12622, Egypt

* Correspondence: mohamed-elgohary@eru.edu.eg (M.K.E.); ha.abdel-aziz@nrc.sci.eg (H.A.A.-A.)

Abstract: Breast cancer is a serious threat to the health and lives of women. Two novel series of *N'*-(2-oxindolin-3-ylidene)-6-methylimidazo[2,1-*b*]thiazole-5-carbohydrazides and 1-(aryl)-3-(6-methylimidazo[2,1-*b*]thiazol-5-yl)ureas were designed, synthesized and investigated for their anti-cancer efficacy against the MCF-7 breast cell line. Three compounds of the first series showed potent activity toward MCF-7 with IC₅₀ in the range 8.38–11.67 μM, respectively, as compared to Sorafenib (IC₅₀ = 7.55 μM). *N'*-(1-butyl-2-oxindolin-3-ylidene)-6-methylimidazo[2,1-*b*]thiazole-5-carbohydrazide inhibited VEGFR-2 with IC₅₀ = 0.33 μM when compared with Sorafenib (IC₅₀ = 0.09 μM). Furthermore, this compound was introduced to PCR assessment, where it increased Bax, caspase 8, caspase 9 and cytochrome C levels by 4.337-, 2.727-, 4.947- and 2.420-fold, respectively, while it decreased levels of Bcl-2, as the anti-apoptotic gene, by 0.359-fold when compared to the untreated control MCF-7. This compound was also arrested in the G2/M phase by 27.07%, compared with 11.31% for the control MCF-7. Furthermore, it induced early and late apoptosis in MCF-7. In addition, a molecular docking study in the VEGFR-2 active site was performed to assess the binding profile for the most active compounds. Moreover, ADME parameters of the targeted compounds were also evaluated.

Keywords: imidazo[2,1-*b*]thiazole; isatin; MCF-7 cell line; VEGFR-2; PCR; cell cycle; apoptosis; molecular docking; ADME



Citation: Alshaye, N.A.; Elgohary, M.K.; Elkotamy, M.S.; Abdel-Aziz, H.A. Design, Synthesis and Biological Assessment of *N'*-(2-Oxindolin-3-ylidene)-6-methylimidazo[2,1-*b*]thiazole-5-carbohydrazides as Potential Anti-Proliferative Agents toward MCF-7 Breast Cancer. *Pharmaceuticals* **2024**, *17*, 216. <https://doi.org/10.3390/ph17020216>

Academic Editor: Abbas G. Shilabin

Received: 15 January 2024

Revised: 1 February 2024

Accepted: 6 February 2024

Published: 7 February 2024



Copyright: © 2024 by the authors. Licensee MDPI, Basel, Switzerland. This article is an open access article distributed under the terms and conditions of the Creative Commons Attribution (CC BY) license (<https://creativecommons.org/licenses/by/4.0/>).

1. Introduction

Cancer is one of the most lethal diseases, and it is rapidly evolving into one of the world's most serious health challenges. Furthermore, the unfavorable side effects of classic non-selective chemotherapies, as well as the growth of resistance to existing chemotherapy medications, make the search for more selective novel cancer fighters a top goal. However, it is difficult to design a drug that prevents the production of aberrant cells with no influence on the exerting of normal cells [1,2]. Pathological angiogenesis, on the flip side, occurs not just in the growth of tumors but additionally in a variety of non-neoplastic conditions [3]. Angiogenesis is also suggested to be linked to a variety of disorders, including cancer [4,5]. The inhibition of angiogenesis may decrease the tumor development because it can slow tumor growth without creating significant negative or resistant effects over time [6]. The VEGF (vascular endothelial growth factor) family members are well-known angiogenic agents that govern blood and lymphatic vessel development and balance in both normal and pathological angiogenesis.

VEGF-A assumes a crucial role in directing vascular development and angiogenesis by interacting with VEGFR-2. The nuanced functions of VEGFR-2 in blood vessel development are supported by adaptor proteins. In the realm of cancer, the secretion of VEGF by cancer cells is instrumental in activating the VEGFR-2 pathway in neighboring endothelial cells, thereby participating in the phenomenon of cancer-related angiogenesis. Notably, the activation of VEGFR-2 signaling has been discerned in breast cancer cells [7–9].

Consequently, VEGFR has been extensively utilized in cancer therapy [10]. VEGF ligands bind to three different tyrosine kinases (VEGFR-TK): FLT-1 (FLT1), FLT-2 (KDR/FLK1) and FLT-4 (FLT4) [11]. VEGFR-2 is activated by the unique binding of VEGF generated by endothelial cells [12] and many malignancies have VEGFR-2 amplification [13]. Series of VEGFR-2 inhibitors have recently been approved for the management of numerous cancers such as Sorafenib (I) [14], Lenvatinib (II) [15] and Sunitinib (III) [16] with IC_{50} = 90, 1 and 10 nM, respectively, as well as urea-based heterocycles IV (IC_{50} = 1.5 μ M) [17] and V (IC_{50} = 6.2 nM) [18] (Figure 1).

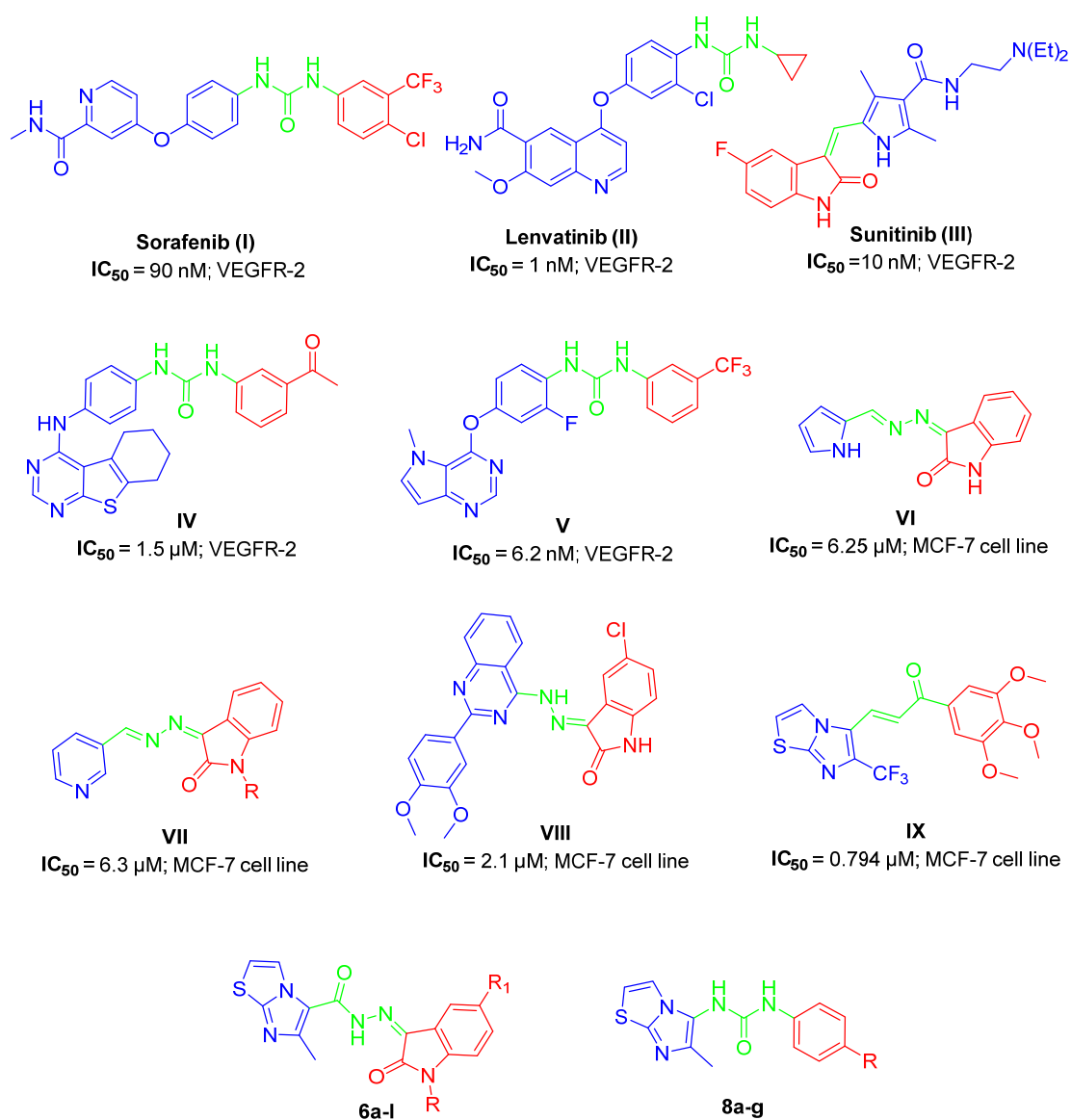


Figure 1. Structure of clinically approved VEGFR-2 inhibitors and some reported anticancer agents (I–IX) with their corresponding IC_{50} values, in addition to our targeted hybrids 6a–l and 8a–g.

The combinations through the hydrazine group, as a linker between position 3 of isatin (indoline-2,3-dione) and certain heterocycles such as pyrrole, pyridine or quinazoline

in compounds **VI** [19], **VII** [20] and **VIII** [21], produce cytotoxic agents against the MCF-7 cancerous cell line with $IC_{50} = 6.25, 6.3$ and $2.1 \mu M$, respectively (Figure 1).

A new class of imidazo[2,1-*b*]thiazoles were developed for anticancer activity and they showed potential activity toward MCF-7 cell line and elicited apoptotic properties such as caspase-9 upregulation; for example, imidazo[2,1-*b*]thiazole derivatives **IX** showed IC_{50} equal to $0.794 \mu M$ on the MCF-7 cell line and were further used for comprehensive biological investigations [22] (Figure 1).

As illustrated in Figure 1, isatin in Sunitinib (**III**) and lead compounds **VI–VIII**, in addition to the imidazo[2,1-*b*]thiazole system in the potent anticancer compound **IX**, are important in the synthesis of potent VEGFR-2 inhibitors and/or MCF-7 anticancer agents. On the other hand, the hydrazine linker in compounds **VI–VIII** and urea bridge in Sorafenib (**I**), Lenvatinib (**II**), **IV** and **V** are critical for the same purpose.

In continuation to our research, which deals with the discovery of novel potent anti-cancer agents [23–28], herein we utilized the fragment linking strategy to construct novel anti-proliferative agents for MCF-7 breast cancer therapy and evaluated their effectiveness on VEGFR enzyme inhibition.

The Sorafenib-VEGFR-2 crystal structure showed the role of the pyridine ring of Sorafenib (**I**) with certain amino acids in the VEGFR-2 hydrophobic pocket [29,30] (Figure 2). However, it is important to understand the SAR of synthetic VEGFR-2 kinase inhibitors [31], which may be a critical factor in determining the efficiency of the agent and its tolerability.

The binding mode of VEGFR-2 inhibitors is characterized by a “head” component that binds to the hinge region and possesses crucial H-bond donor and/or acceptor capabilities for interacting with Cys919. Additionally, they have a “linker” spanning three to four chemical bonds with H-bonding moiety to establish the interactions with Asp1046. Furthermore, they have a “tail” segment containing a hydrophobic moiety that occupies the allosteric hydrophobic back pocket [32–34].

In this context, we developed two sets of *N'*-(2-oxoindolin-3-ylidene)-6-methylimidazo thiazole-5-carbohydrazides **6a–I** and 1-(aryl)-3-(6-methylimidazo[2,1-*b*]thiazol-5-yl)ureas **8a–g** (Figures 1 and 2). Regarding the binding pocket of Sorafenib (**I**), the pyridine residue was specifically linked with Leu1035, Phe1047, Val848, Val916 and Cys1045 through various forms of interactions in the hinge region, whereas the H interaction was preserved via the urea linker with Asp1046. Furthermore, Leu889 and Glu885 maintained the link between the substituted phenyl ring through distinct interactions (Figure 2). Therefore, the aimed structures **6a–I** were designed according to the fragment combination approach, as follows: the 6-methylimidazo[2,1-*b*]thiazole system replaced the 4-phenoxy pyridine moiety in the left side of Sorafenib (**I**), whereas the isatin moiety with several substitution patterns in position 1 and/or 5 replaced the aryl group of the right side of Sorafenib (**I**) with a carbohydrazide linker (H-bond acceptor–H-bond donor linker) similar to the urea bridge in Sorafenib (**I**) in order to obtain an activity similar or higher to that of Sorafenib (**I**) (Figure 2). We also followed the same approach to design urea derivatives **8a–g** (Figure 2). The latter two sets were synthesized and evaluated toward MCF-7 cell cytotoxicity. The most potent compounds were introduced to examine their activity toward VEGFR-2, PCR assessment, apoptosis and cell cycle analysis.

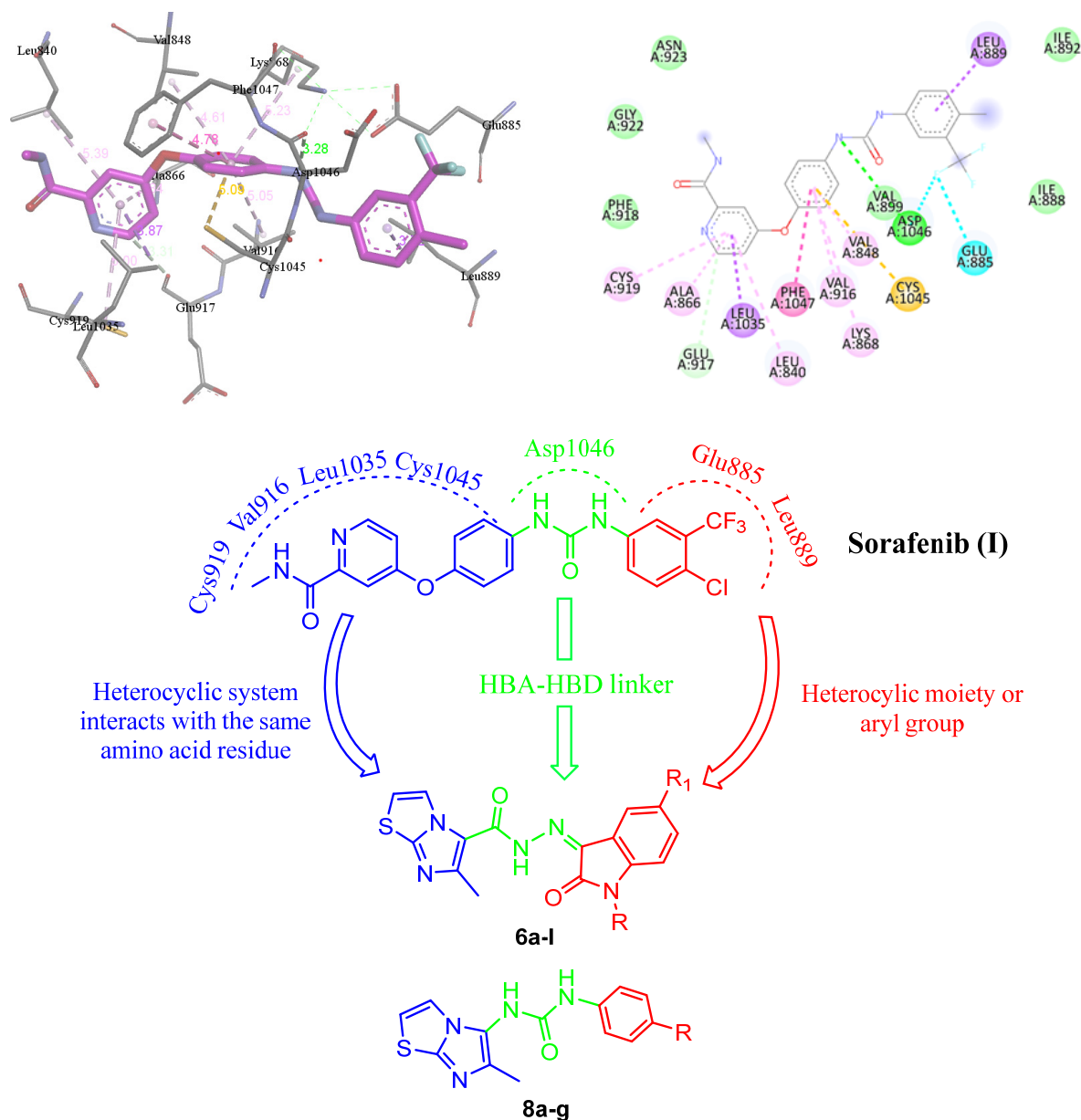


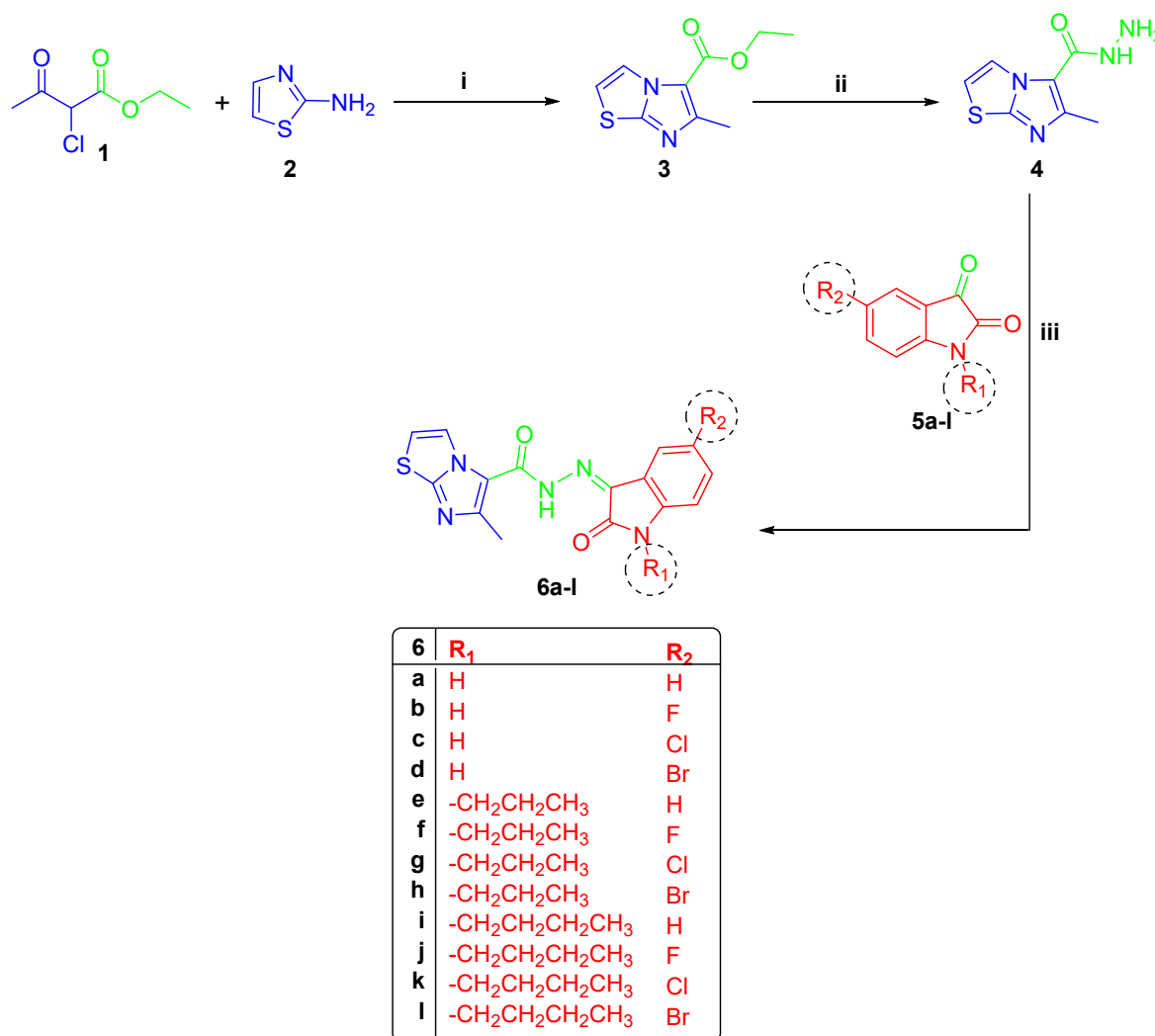
Figure 2. Docking of Sorafenib (I) with VEGFR-2 binding site and the assumed possible modifications of the targeted structures 6a-l and 8a-g.

2. Results and Discussion

2.1. Chemistry

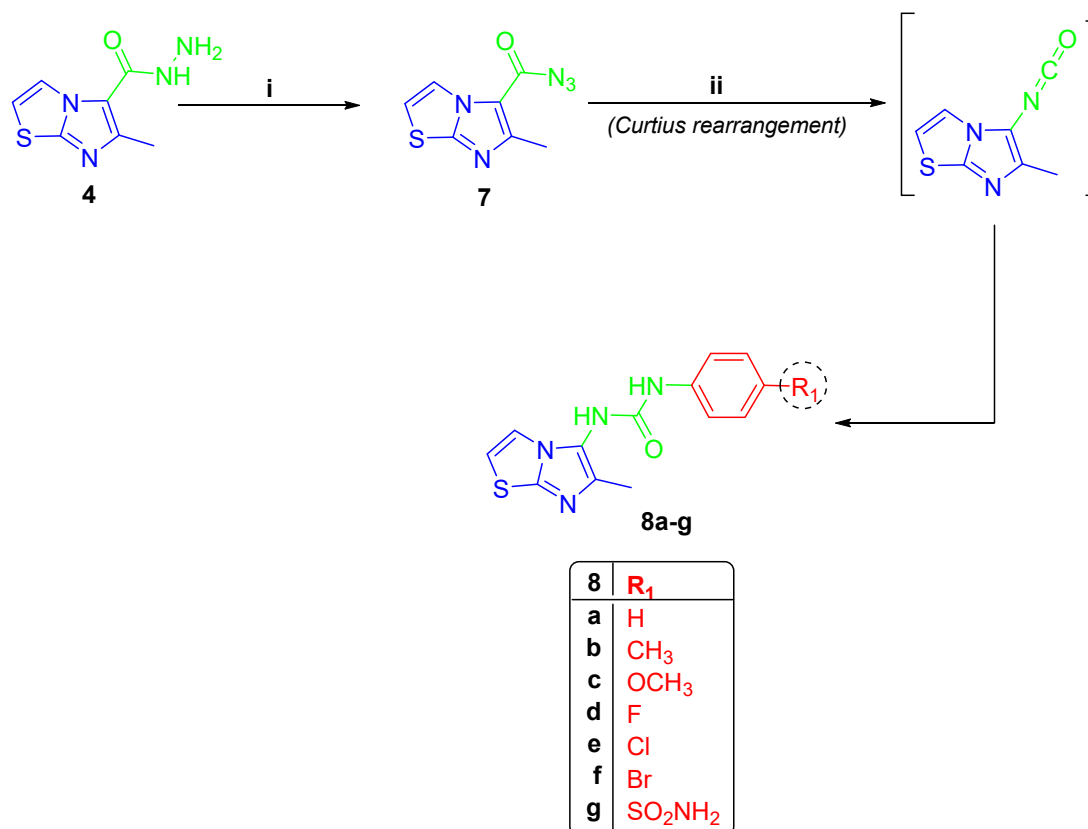
The reaction of 2-chloroethylacetoacetate (1) with 2-aminothiazole (2), in 1,2-dimethoxyethane at 90 °C, yielded the key ester 3. Under reflux circumstances, the latter ester was transformed into acid hydrazide 4 using 99% hydrazine hydrate [29]. Subsequently, compound 4 was reacted with several substituted indoline-2,3-dione derivatives 5a-l to yield the target 6-methyl-*N'*-(2-oxo-substituted/ unsubstituted-indolin-3-ylidene) imidazo[2,1-*b*]thiazole-5-carbohydrazides 6a-l (Scheme 1). The ¹H NMR data of compounds 6a-d revealed three distinct signals, one around 2.65 ppm for CH₃ of imidazo thiazole and two D₂O exchangeable signals around 11.30 and 13.26 ppm for isatin NH and carbohydrazide NH, respectively. Compounds 6e-h with *n*-propyl substitution in position 1 showed three aliphatic signals of the -CH₂-CH₂-CH₃ group around 0.90, 1.55–1.70 and 3.70 ppm, in addition to a singlet CH₃ of imidazo[2,1-*b*]thiazole around 2.75 ppm. They also showed a D₂O exchangeable hydrazide NH signal around 13.20 ppm. Furthermore,

butyl-substituted compounds **6i–l** were characterized with five aliphatic distinguishing signals arising in the same highlights as prior propyl compounds with an extra multiplet peak of CH₂, in addition to the signal of imidazo[2,1-*b*]thiazole CH₃. Concerning ¹³C NMR, spectra of **6a–l** exhibited distinct signal around 16.45 ppm for the CH₃ group of imidazothiazole moiety. Moreover, ¹³C NMR of **6e–h** revealed three signals around 11.50, 28.82 and 42.22 ppm for the *n*-propyl group; on the other hand, compounds **6i–l** revealed four separate signals around 13.91, 20.00, 30.30 and 40.80 ppm for *n*-butyl substitution (Figures S4–S19, Supplementary Data).



Scheme 1. (i) 1,2-dimethoxyethane, ref., 6 h; (ii) N₂H₄·H₂O/ethanol, ref., 3 h; (iii) EtOH/glacial acetic acid, reflux 4 h.

On the other hand, compound **4** was subjected to a *Citrous* rearrangement process by its reaction with NaNO₂ and HCl to obtain azide **7** [30] which was then refluxed in dioxane with various anilines to yield urea derivatives **8a–g** (Scheme 2). The ¹H NMR spectra of compounds **8a–g** revealed three signals, one around 2.12 ppm for CH₃ protons and the remaining two signals around 8.16 ppm and 9.02 ppm for two D₂O exchangeable NH protons of the urea linker. Compound **8g** was characterized with an additional D₂O exchangeable signal of sulphonamide NH₂ at 7.17 ppm. The existence of two separate signals around 13.37 ppm and 154.20 ppm for the CH₃ and carbonyl groups was seen in ¹³C NMR spectra of **8a–g**. The ¹H NMR of compounds **8b** and **8c** showed the signals of -CH₃ and -OCH₃ protons, respectively, and the appearance of their carbon signals in ¹³C NMR (Figures S20–S33, Supplementary Data).



Scheme 2. (i) NaNO₂/HCl/ H₂O, stirring 3 h; (ii) dioxane/diff. anilines, reflux 8 h.

2.2. Anticancer Activity

2.2.1. Cytotoxicity of the Designed Compounds 6a–l and 8a–g on MCF-7 and MCF-10A

The anti-cancer potency of **6a–l** and **8a–g** was investigated towards the MCF-7 breast cell line using MTT assay and their IC₅₀ values were determined, compared to Sorafenib (**I**) [35]. The majority of the compounds **6a–l** and **8a–g** have a wide range of activity against the MCF-7 cell line, with IC₅₀ ranging from 23.97 ± 0.67 μM for **6a** to 114.61 ± 4.99 μM for **8b** comparing with Sorafenib (**I**) (IC₅₀ = 7.55 ± 0.40 μM) (Table 1). On the other side, compounds **6b**, **6i** and **6j** showed potent anticancer activity toward MCF-7 cell lines, with IC₅₀ = 11.50 ± 0.52, 8.38 ± 0.62 and 11.67 ± 0.52 μM, respectively, as compared to Sorafenib (**I**) (IC₅₀ = 7.55 ± 0.40 μM) (Table 1).

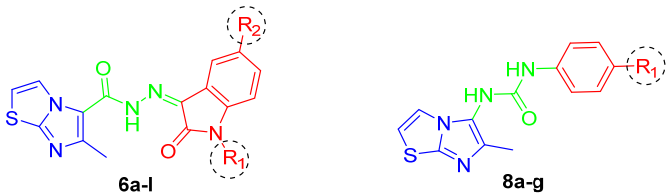
On the other hand, compounds **6b**, **6i** and **6j** revealed non-cytotoxic activity toward MCF-10A due to its non-tumorigenic origin [36], where their IC₅₀ = 125.26 ± 2.7, 54.63 ± 1.29 and 47.73 ± 0.53 μM, when compared to Sorafenib (IC₅₀ = 22.35 ± 1.29 μM) (Table 2).

2.2.2. SARs of Compounds 6a–l and 8a–g on MCF-7 Cell Line

SARs assessments of the aforementioned data of compounds **6a–l** revealed that the linking between the imidazo[2,1-*b*]thiazole system and indoline-2,3-dione via the hydrazide bridge showed a wide range of activity as **6c**, **6e**, **6f**, **6g**, **6h**, **6k** and **6l** have weak antiproliferative activity, with an IC₅₀ range of 43.10 ± 3.69–82.55 ± 2.75 μM in comparison to Sorafenib (**I**) (IC₅₀ = 7.55 ± 0.40 μM), while compounds **6a** (IC₅₀ = 23.97 ± 0.67 μM) and **6d** (IC₅₀ = 22.80 ± 1.38 μM) revealed moderate anti-proliferative activity. Regarding **6b**, **6i** and **6j**, they showed the highest anticancer activity with an IC₅₀ range = 8.38 ± 0.62–11.67 ± 0.52 μM. *N'*-(1-butyl-2-oxindolin-3-ylidene)-6-methylimidazo[2,1-*b*]thiazole-5-carbohydrazide (**6i**) with *n*-butyl substitution (R = *n*-butyl) in position 1 of isatin moiety exhibited the highest anticancer activity (IC₅₀ = 8.38 ± 0.62 μM), followed by **6b** with fluoro-substitution (R₁ = F) in position 5 of isatin moiety, with an IC₅₀ = 11.50 ± 0.52 μM, whereas compound **6j** with

n-butyl substitution ($R_1 = n$ -butyl) and fluoro-substitution ($R_2 = F$) in positions 1 and 5 of isatin moiety, respectively, had an IC_{50} range = $11.67 \pm 0.52 \mu M$ (Table 1). From the latter data, the variation in substitutions in positions 1 and 5 of isatin moiety plays an important role in the anticancer activity of hybrids **6a–l**; for example, the impact of F is higher than Cl or Br, whereas the effect of *n*-butyl substitution is higher than that of *n*-propyl. On the other side, imidazo[2,1-*b*]thiazoles with arylurea branch compounds **8a–g** showed anticancer activities lower than those of **6a–l**.

Table 1. Anti-proliferative activity of **6a–l** and **8a–g** toward MCF-7 cell line.



Compound	R_1	R_2	IC_{50} (μM)
6a	H	H	23.97 ± 0.67
6b	H	F	11.50 ± 0.52
6c	H	Cl	43.10 ± 3.69
6d	H	Br	22.80 ± 1.38
6e	<i>n</i> -propyl	H	61.39 ± 3.15
6f	<i>n</i> -propyl	F	82.55 ± 2.75
6g	<i>n</i> -propyl	Cl	52.47 ± 1.26
6h	<i>n</i> -propyl	Br	74.34 ± 2.19
6i	<i>n</i> -butyl	H	8.38 ± 0.62
6j	<i>n</i> -butyl	F	11.67 ± 0.52
6k	<i>n</i> -butyl	Cl	42.72 ± 2.01
6l	<i>n</i> -butyl	Br	52.55 ± 2.36
8a	H	–	109.68 ± 4.62
8b	CH ₃	–	114.61 ± 4.99
8c	OCH ₃	–	106.43 ± 5.32
8d	F	–	72.33 ± 4.71
8e	Cl	–	35.72 ± 3.32
8f	Br	–	31.12 ± 2.47
8g	SO ₂ NH ₂	–	41.57 ± 1.59
Sorafenib (I)	–	–	7.55 ± 0.40

Table 2. IC_{50} values of **6b**, **6i** and **6j** toward MCF-10A.

Compound	IC_{50} (μM)
6b	125.26 ± 2.7
6i	54.63 ± 1.29
6j	47.73 ± 0.53
Sorafenib (I)	22.35 ± 1.29

2.2.3. VEGFR-2 Inhibitory Activity (IC_{50}) for Compounds **6b**, **6i** and **6j**

The VEGFR-2 inhibitory activity for compounds **6b**, **6i** and **6j** was investigated and the results in IC_{50} computed from the concentration–inhibition response curve compared to Sorafenib (I) are summarized in Table 3. The VEGFR-2 inhibitory effects of **6b**, **6i** and **6j**, respectively, showed good activity, with an $IC_{50s} = 3.85 \pm 0.15$, 0.33 ± 0.01 and $1.51 \pm 0.06 \mu M$, respectively, when compared to Sorafenib (I) ($IC_{50} = 0.09 \pm 0.004 \mu M$). Compound **6j** ($IC_{50} = 1.51 \pm 0.06 \mu M$) displayed a significant influence on kinase activity when compared to **6b** with $IC_{50} = 3.85 \pm 0.15 \mu M$, which indicated the effect of positions 1 and 5 substitutions of isatin moiety. However, compound **6j** revealed the highest VEGFR-2 inhibition activity, with $IC_{50} = 0.33 \pm 0.01 \mu M$.

Table 3. In vitro VEGFR-2 inhibitory activity for **6b**, **6i** and **6j**.

Compounds	R ₁	R ₂	IC ₅₀ (μM)
6b	H	F	3.85 ± 0.15
6i	<i>n</i> -butyl	H	0.33 ± 0.01
6j	<i>n</i> -butyl	F	1.51 ± 0.06
Sorafenib (I)	–	–	0.09 ± 0.004

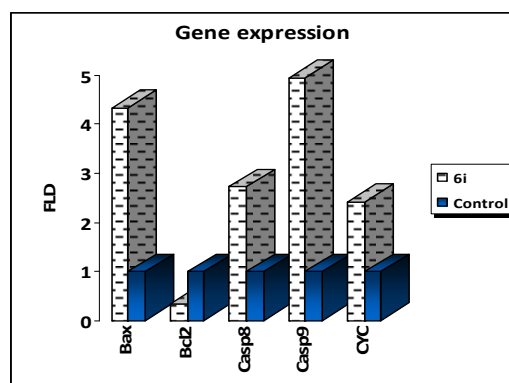
2.2.4. PCR Assessment for Compound **6i**

The gene expression levels of apoptosis genes in MCF-7 cells were measured using RT-PCR to validate the apoptosis-inducing behaviors of the potent lead compound **6i** in MCF-7 cells. Compound **6i** increased Bax levels by 4.337-fold, caspase 8 levels by 2.727-fold, caspase 9 levels by 4.947-fold and cytochrome C levels by 2.420-fold, while it decreased the level of Bcl-2, as the anti-apoptotic gene, by 0.359-fold when compared to the untreated control MCF-7 (Table 4).

Table 4. Fold change of apoptosis genes in treated MCF-7 cells with **6i**.

	RT-PCR Fold Change				
	Bax	Caspase-8	Caspase-9	Cytochrome C	Bcl-2
6i /MCF-7	4.337	2.727	4.947	2.420	0.359
Control MCF-7	1	1	1	1	1

The results revealed an inherent apoptotic mechanism including the activation of Bax, cytochrome C, and caspases 3 and 9. As a result, our RT-PCR findings supported prior research by demonstrating that the apoptotic pathway is characterized by the overexpression of proapoptotic genes and the downregulation of anti-apoptotic genes (Figure 3).

**Figure 3.** Quantitative RT-PCR results analysis of the apoptosis-related genes, cytochrome, Bax, Caspases 8, 9 and Bcl-2, in **6i**-treated MCF-7 cells. Dashed line represents the gene expression for potent **6i** and blue line represents untreated control.

2.2.5. Cell Cycle Analysis of Compound **6i** on MCF-7

Compound **6i** arrested cells in the G2/M phase with %G2/M = 27.07, compared with %G2/M = 11.31 for the control MCF-7 (Table 5 and Figure 4).

Table 5. Cell cycle of compound **6i** in MCF-7.

	%G0-G1	%S	%G2/M
6i /MCF-7	53.66	19.27	27.07
Cont. MCF-7	64.73	23.96	11.31

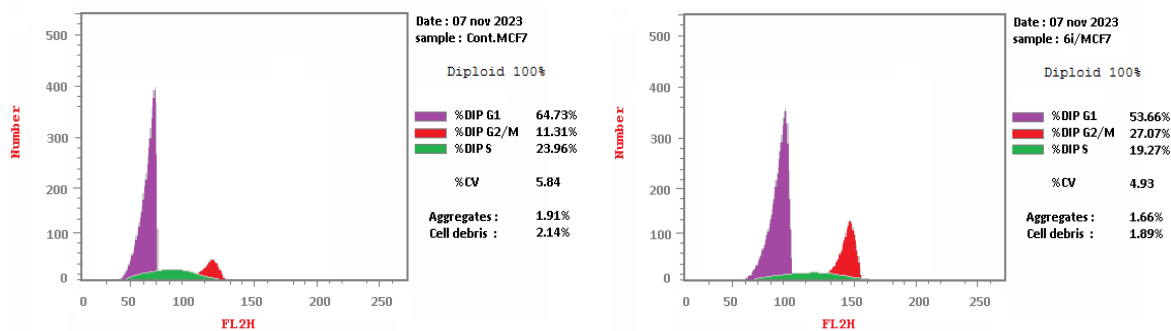


Figure 4. Cell cycle for cont. MCF-7 (left) and 6i (right).

2.2.6. Apoptotic Assay for Compound 6i

In comparison to the control cells, the apoptotic assay employing Annexin V/PI analysis for compound 6i generated a substantial amount of early and late apoptosis in MCF-7. Compound 6i induced early apoptosis in MCF-7 at rate of 22.05, compared with the control MCF-7 (0.43) (Table 6 and Figure 5). Furthermore, 6i demonstrated late apoptosis at rate 7.61 compared with the control MCF-7 (0.11).

Table 6. Apoptosis analysis for 6i in MCF-7.

	Total	Early	Late	Necrosis
6i/MCF-7	32.81	22.05	7.61	3.15
Cont. MCF-7	1.91	0.43	0.11	1.37

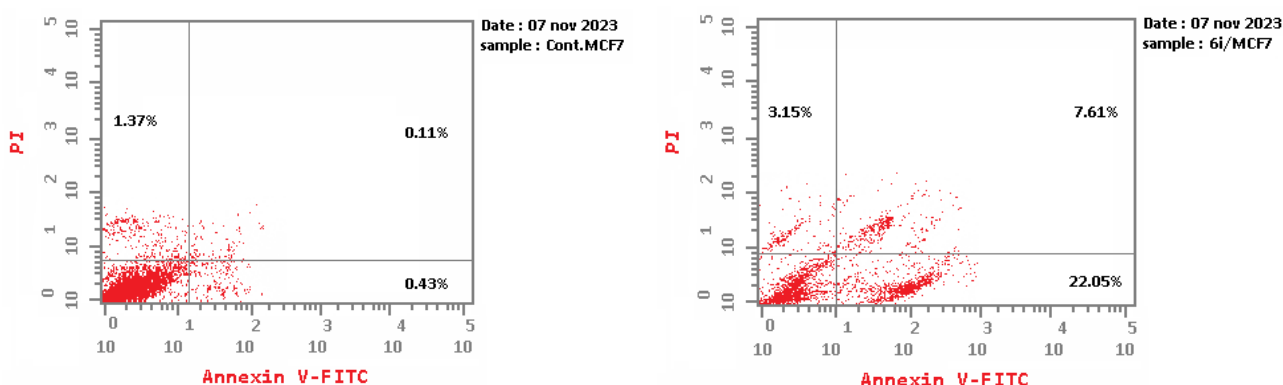


Figure 5. Apoptosis analysis for control MCF-7 (left) and 6i (right).

2.3. Molecular Modeling Study

The computational docking method is used for approximating two fundamental concepts. The main objective is to determine the correct spot and orientation of a particular chemical pose in the binding site of the enzyme. The second concept is the calculation of docking score (the strength of protein-ligand interactions) [37]. In an attempt to explain the cytotoxic action of 6b, 6i and 6j, a docking study in the VEGFR-2 active site was performed. Redocking of sorafenib (I) in the active site of VEGFR-2 (PDB: 4ASD) was nearly in the exact position as the co-crystallized ligand with d. s. = -10.6 kcal/mol (Figure S1, Supplementary Data).

The docking investigation of 6b, 6i and 6j in the VEGFR-2 active site revealed binding mechanisms that were similar to the lead medicine and they showed docking scores that were higher or comparable to the docked lead. The hot areas were satisfied by targeted compounds, which established H-bonds with Cys919, Glu885 and Asp1046 residues which helped to explain the substantial VEGFR-2 inhibitory effect, as shown in Figure 6.

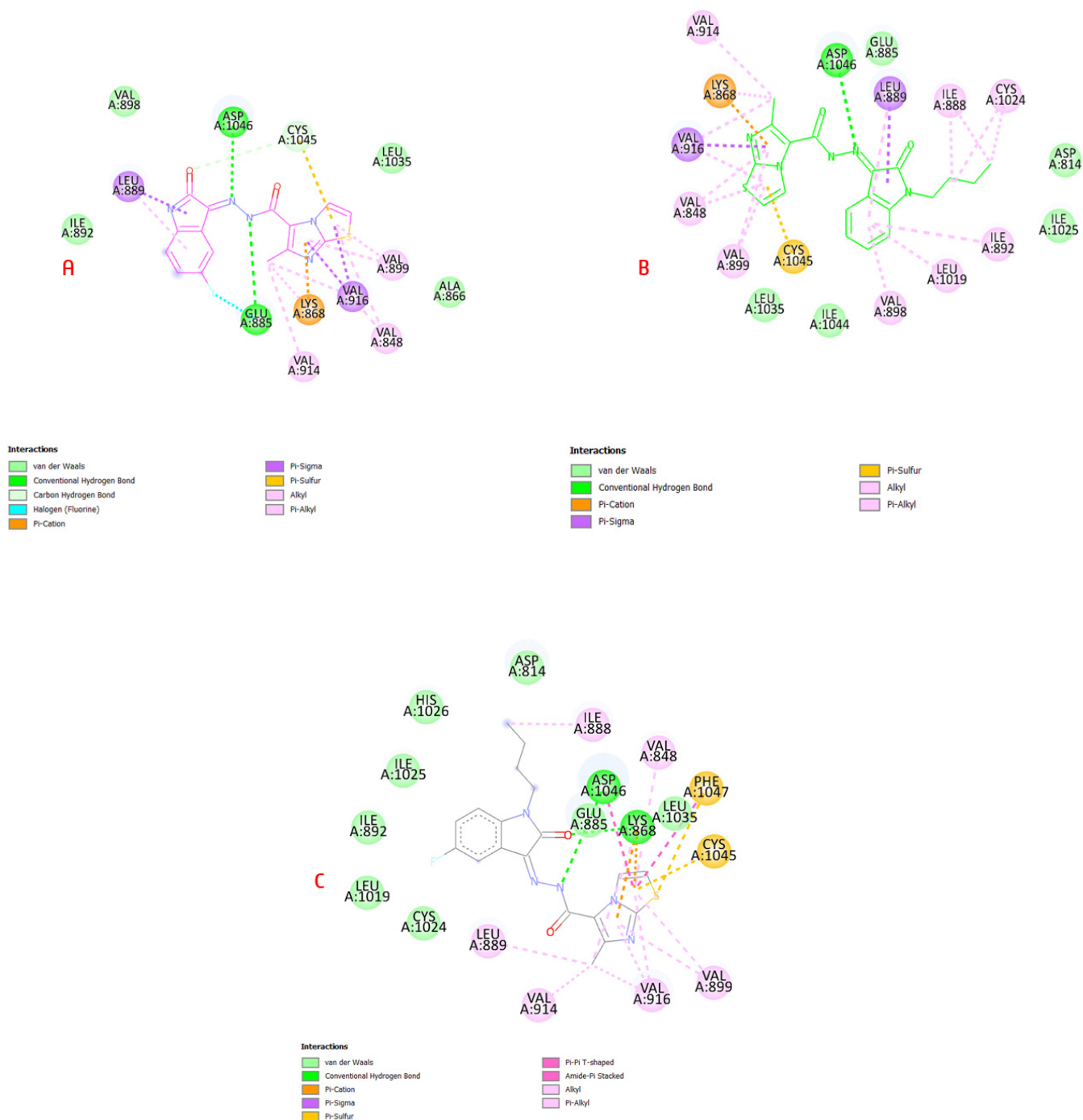


Figure 6. (A) **6b** in VEGFR-2 binding site showed H-bond with Asp1046 and pi-cation interaction with Lys868; (B) compound **6i** revealed H-bond with Asp1046, pi-sigma interaction with Cys1045 and pi-cation interaction with Lys868; (C) **6j** showed H-interactions with Asp1046 and Lys868 residues (Table S1, Supplementary Data).

As shown in the interactions of **6b**, **6i** and **6j** on the VEGFR-2 active site, they interacted with the same pattern of sorafenib (**I**) with a hydrogen-bond interaction with amino acid Asp1046 via the linker hydrazide moiety, while imidazothiazole bonded with Val916 and Cys1045 as the pyridine side; on the other hand, phenyl isatin bonded with Leu889 via pi-sigma as the substituted phenyl in the Sorafenib (**I**) structure (Figure S2, Supplementary Data).

2.4. Computational ADME Study

Three rules, at least, of the following five rules are requested for oral bioavailability: There are no more than five H-bond donors, no more than 500 Da MWt, no more than five log P, only one violation and no more than ten H-bond acceptors, according to Lipinski's rule of five [38]. The Veber rule predicts that molecules with less than 10 rotatable bonds and at least 140.2 of polar surface area will have appropriate oral bioavailability [39]. ADME parameters of the targeted compounds **6a–l** and **8a–g** such as the proportion of human intestinal absorption and blood–brain barrier penetration were evaluated using the SWISSADME method. Their BBB penetration was expected to be minimal, which prevents these candidates from passing the BBB or having harmful effects on the central nervous system (Figure S3 and Table S2, Supplementary Data).

3. Materials and Methods

3.1. Chemistry

The specifications of instruments used in the chemistry part are listed in the Supplementary Data, page 42.

3.1.1. Preparation of Carbohydrazide **4**

A mixture of 2-aminothiazole (**1**) (10.0 g, 100 mmol) and ethyl 2-chloroacetoacetate (**2**) (16.5 g, 100 mmol) was refluxed for 6 h in 1,2-dimethoxyethane (50 mL). After evaporation of the solvent, off-white precipitate was formed and then recrystallized from EtOH to afford compound **3**. The latter ester **3** (2.10 g, 10 mmol) was treated with hydrazine hydrate (99%, 2 mL) for 4 h in refluxed EtOH (50 mL). The solvent was evaporated to obtain white precipitate, which then recrystallized from EtOH to give carbohydrazide **4** [40].

3.1.2. Synthesis of Hybrids **6a–l**

A mixture of carbohydrazide **4** (0.196 g, 1.0 mmol) and indoline-2,3-dione derivatives **5a–l** (1.0 mmol) in EtOH (30 mL) and AcOH (0.3 mL) was refluxed for 4 h. Crystallization of the resulting solid from EtOH/DMF gave compounds **6a–l**, respectively.

6-Methyl-*N'*-(2-oxoindolin-3-ylidene)imidazo[2,1-*b*]thiazole-5-carbohydrazide (**6a**)

Yield = 68%; m.p. = >300 °C; IR: 1697 (>C=O), 3263 (>N-H), 3444 (>N-H); ¹H NMR: 2.65 (s, 3H, -CH₃), 6.92 (d, *J* = 8.1 Hz, 1H, Ar-H), 7.07 (d, *J* = 8.1 Hz, 1H, Ar-H), 7.31–7.36 (m, 1H, Ar-H), 7.41 (d, *J* = 4.5 Hz, 1H, Ar-H), 7.53 (d, *J* = 7.5 Hz, 1H, Ar-H), 8.21 (d, *J* = 4.5 Hz, 1H, Ar-H), 11.11 (s, 1H, >N-H), 13.26 (s, 1H, >N-H); ¹³C NMR: 16.88 (-CH₃), 111.73, 115.41, 117.66, 120.61, 121.22, 121.74, 132.04, 137.52, 142.82, 148.80, 152.63, 157.08 (>C=O), 163.16 (>C=O); Anal. for C₁₅H₁₁N₅O₂S (325.35): calcd.: C, 55.38; H, 3.41; N, 21.53; found: C, 55.50; H, 3.47; N, 21.37.

N'-(5-Fluoro-2-oxoindolin-3-ylidene)-6-methylimidazo[2,1-*b*]thiazole-5-carbohydrazide (**6b**)

Yield = 74%; m.p. = >300 °C; IR: 1710 (>C=O), 3294 (>N-H), 3420 (>N-H); ¹H NMR: 2.65 (s, 3H, -CH₃), 6.93 (q, *J* = 4.0 Hz, 1H, Ar-H), 7.15–7.19 (m, 1H, Ar-H), 7.33 (dd, *J* = 8.1 Hz, 1H, Ar-H), 7.42 (d, *J* = 4.1 Hz, 1H, Ar-H), 8.22 (d, *J* = 4.0 Hz, 1H, Ar-H), 11.14 (s, 1H, >N-H), 13.28 (s, 1H, >N-H); ¹³C NMR: 16.89 (-CH₃), 40.73, 108.34, 112.85, 115.54 (2C), 117.59, 118.29, 121.75 (2C), 139.05, 149.06, 152.81, 157.01 (>C=O), 163.29 (>C=O); Anal. for C₁₅H₁₀FN₅O₂S (343.34): calcd.: C, 52.47; H, 2.94; N, 20.40; found: C, 52.21; H, 2.99; N, 20.53.

N'-(5-Chloro-2-oxoindolin-3-ylidene)-6-methylimidazo[2,1-*b*]thiazole-5-carbohydrazide (**6c**)

Yield = 67%; m.p. = 292–293 °C; IR: 1705 (>C=O), 3124 (>N-H), 3367 (>N-H); ¹H NMR: 2.68 (s, 3H, -CH₃), 6.95 (d, *J* = 8.5 Hz, 1H, Ar-H), 7.39 (d, *J* = 4.0 Hz, 1H, Ar-H), 7.48 (d, *J* = 4.0 Hz, 1H, Ar-H), 7.51 (m, 1H, Ar-H), 8.26 (d, *J* = 4.4 Hz, 1H, Ar-H), 11.38 (s, 1H, >N-H), 13.26 (s, 1H, >N-H); ¹³C NMR: 16.91 (-CH₃), 113.25, 115.53, 117.56, 120.67, 121.75, 122.31, 127.42, 131.39, 136.48, 141.44, 149.03, 152.80, 156.92 (>C=O), 162.94 (>C=O); Anal.

for $C_{15}H_{10}ClN_5O_2S$ (359.79): calcd.: C, 50.08; H, 2.80; N, 19.47; found: C, 49.91; H, 3.01; N, 19.50.

N'-(5-Bromo-2-oxoindolin-3-ylidene)-6-methylimidazo[2,1-*b*]thiazole-5-carbohydrazide (**6d**)

Yield = 66%; m.p. = 296–297 °C; IR: 1705 (>C=O), 3116 (>N-H), 3383 (>N-H); 1H NMR: 2.62 (s, 3H, -CH₃), 6.85 (s, 1H, Ar-H), 7.42–7.46 (m, 2H, Ar-Hs), 7.56 (s, 1H, Ar-H), 8.20 (s, 1H, Ar-H), 11.33 (s, 1H, >N-H), 13.20 (s, 1H, >N-H); ^{13}C NMR: 13.36 (-CH₃), 112.07 (2C), 115.59, 115.76 (2C), 118.58, 118.98, 1120.82, 136.62, 137.29, 144.84, 154.29, 156.98 (C=O), 158.87 (C=O); Anal. for $C_{15}H_{10}BrN_5O_2S$ (404.24): calcd.: C, 44.57; H, 2.49; N, 17.33; found: C, 44.30; H, 2.36; N, 17.37.

6-Methyl-*N'*-(2-oxo-1-propylindolin-3-ylidene)imidazo[2,1-*b*]thiazole-5-carbohydrazide (**6e**)

Yield = 51%; m.p. = 256–257 °C; IR: 1702 (>C=O), 3236 (>N-H); 1H NMR: 0.89 (t, $J = 7.5$ Hz, 3H, -CH₃), 1.62–1.69 (m, 2H, >CH₂), 2.67 (s, 3H, -CH₃), 3.71 (t, $J = 7.5$ Hz, 2H, >CH₂), 7.12–7.19 (m, 2H, Ar-Hs), 7.41–7.44 (m, 2H, Ar-Hs), 7.59 (d, $J = 8.1$ Hz, 1H, Ar-H), 8.22 (d, $J = 4.0$ Hz, 1H, Ar-H), 13.21 (s, 1H, >N-H); ^{13}C NMR: 11.55 (-CH₃), 17.03 (-CH₃), 28.89 (>CH₂), 41.65 (>CH₂), 112.80, 113.01, 115.65, 121.82, 123.48, 134.33, 135.65, 142.20, 148.27, 152.71, 156.25, 161.10 (>C=O); Anal. for $C_{18}H_{17}N_5O_2S$ (367.43): calcd.: C, 58.84; H, 4.66; N, 19.06; found: C, 59.07; H, 4.59; N, 19.20.

N'-(5-Fluoro-2-oxo-1-propylindolin-3-ylidene)-6-methylimidazo[2,1-*b*]thiazole-5-carbohydrazide (**6f**)

Yield = 66%; m.p. = 243–244 °C; IR: 1689 (>C=O), 3224 (>N-H); 1H NMR: 0.92 (t, $J = 7.5$ Hz, 3H, -CH₃), 1.64–1.70 (m, 2H, >CH₂), 2.72 (s, 3H, -CH₃), 3.76 (t, $J = 7.5$ Hz, 2H, >CH₂), 7.26–7.32 (m, 2H, Ar-Hs), 7.43–7.45 (m, 1H, Ar-H), 7.48 (d, $J = 4.4$ Hz, 1H, Ar-H), 8.38 (s, 1H, Ar-H), 13.21 (s, 1H, >N-H); ^{13}C NMR: 11.51 (-CH₃), 17.20 (-CH₃), 29.90 (>CH₂), 41.71 (>CH₂), 113.21, 113.29, 114.50, 123.18, 125.58, 132.10, 134.23, 143.60, 149.55, 153.79, 156.63, 162.12 (>C=O); Anal. for $C_{18}H_{16}FN_5O_2S$ (385.42): calcd.: C, 56.09; H, 4.18; N, 18.17; found: C, 55.82; H, 4.21; N, 18.30.

N'-(5-Chloro-2-oxo-1-propylindolin-3-ylidene)-6-methylimidazo[2,1-*b*]thiazole-5-carbohydrazide (**6g**)

Yield = 61%; m.p. = 254–255 °C; IR: 1693 (>C=O), 3236 (>N-H); 1H NMR: *E/Z*, 0.83, 0.87 (2t, $J = 7.0$ Hz, $J = 7.5$ Hz, 3H, -CH₃), 1.54–1.63 (2m, 2H, >CH₂), 2.52, 2.68 (2s, 3H, -CH₃), 3.66, 3.72 (2t, $J = 7.0$ Hz, $J = 7.5$ Hz, 2H, >CH₂), 7.18, 7.26 (2d, $J = 8.5$ Hz, $J = 9.0$ Hz, 1H, Ar-H), 7.39–7.45 (2d, $J = 4.0$ Hz, $J = 4.4$ Hz, 1H, Ar-H), 7.48–7.55 (m, 2H, Ar-Hs), 8.18, 8.25 (2s, 1H, Ar-H), 11.46, 13.20 (2s, 1H, >N-H); ^{13}C NMR: 11.43 (-CH₃), 16.30 (-CH₃), 28.40 (>CH₂), 43.51 (>CH₂), 112.56, 113.65, 118.58, 124.29, 124.52, 132.18, 134.23, 144.64, 149.05, 154.59, 155.83, 162.23 (>C=O); Anal. for $C_{18}H_{16}ClN_5O_2S$ (401.87): calcd.: C, 53.80; H, 4.01; N, 17.43; found: C, 53.53; H, 3.84; N, 17.57.

N'-(5-Bromo-2-oxo-1-propylindolin-3-ylidene)-6-methylimidazo[2,1-*b*]thiazole-5-carbohydrazide (**6h**)

Yield = 50%; m.p. = 261–262 °C; IR: 1724 (>C=O), 3232 (>N-H); 1H NMR: *E/Z*, 0.83, 0.86 (2t, $J = 7.0$ Hz, $J = 7.5$ Hz, 3H, -CH₃), 1.54–1.63 (2m, 2H, >CH₂), 2.36, 2.66 (2s, 3H, -CH₃), 3.65, 3.69 (2t, $J = 7.0$ Hz, $J = 7.5$ Hz, 2H, >CH₂), 7.12, 7.18 (2d, $J = 8.5$ Hz, $J = 9.0$ Hz, 1H, Ar-H), 7.38, 7.44 (2d, $J = 4.0$ Hz, $J = 4.5$ Hz, 1H, Ar-H), 7.57–7.64 (m, 2H, Ar-Hs), 8.06, 8.23 (2d, $J = 4.0$ Hz, $J = 5.0$ Hz, 1H, Ar-H), 11.14, 13.60 (2s, D₂O exchangeable, 1H, >N-H); ^{13}C NMR: 11.58 (-CH₃), 17.00 (-CH₃), 28.87 (>CH₂), 41.60 (>CH₂), 112.75, 115.47, 115.60, 121.78, 123.28, 134.10, 135.43, 142.50, 149.17, 152.89, 156.92, 161.04 (>C=O); Anal. for $C_{18}H_{16}BrN_5O_2S$ (446.32): calcd.: C, 48.44; H, 3.61; N, 15.69; found: C, 48.56; H, 3.53; N, 15.71.

N'-(1-Butyl-2-oxoindolin-3-ylidene)-6-methylimidazo[2,1-*b*]thiazole-5-carbohydrazide (**6i**)

Yield = 45%; m.p. = 250–251 °C; IR: 1670 (>C=O), 3240 (>N-H); 1H NMR: 0.92 (t, $J = 7.2$ Hz, 3H, -CH₃), 1.35–1.39 (m, 2H, >CH₂), 1.60–1.66 (m, 2H, >CH₂), 2.73 (s, 3H, -CH₃),

3.79 (t, $J = 7.3$ Hz, 2H, >CH₂), 7.17–7.24 (m, 2H, Ar-Hs), 7.45–7.49 (m, 2H, Ar-Hs), 7.64 (d, $J = 7.2$ Hz, 1H, Ar-H), 8.34 (s, 1H, Ar-H); ¹³C NMR: 14.02 (-CH₃), 16.97 (-CH₃), 20.04 (>CH₂), 29.64 (>CH₂), 39.24 (>CH₂), 40.77, 42.23, 110.65, 115.48, 117.63, 120.02, 121.06, 121.76, 123.66, 132.02, 136.63, 143.38, 148.91, 161.32 (>C=O); Anal. for C₁₉H₁₉N₅O₂S (381.45): calcd.: C, 59.83; H, 5.02; N, 18.36; found: C, 59.67; H, 4.85; N, 18.39.

N'-(1-Butyl-5-fluoro-2-oxoindolin-3-ylidene)-6-methylimidazo[2,1-*b*]thiazole-5-carbohydrazide (**6j**)

Yield = 50%; m.p. = 237–238 °C; IR: 1670 (>C=O), 3244 (>N-H); ¹H NMR: 0.86 (t, $J = 7.0$ Hz, 3H, -CH₃), 1.26–1.33 (m, 2H, >CH₂), 1.53–1.59 (m, 2H, >CH₂), 2.66 (s, 3H, -CH₃), 3.71 (t, $J = 7.5$ Hz, 2H, >CH₂), 7.17–7.20 (m, 1H, Ar-H), 7.23–7.27 (m, 1H, Ar-H), 7.37 (d, $J = 8.1$ Hz, 1H, Ar-H), 7.44 (d, $J = 4.0$ Hz, 1H, Ar-H), 8.22 (d, $J = 4.0$ Hz, 1H, Ar-H), 13.20 (s, 1H, >N-H); ¹³C NMR: 14.00 (-CH₃), 16.97 (-CH₃), 20.01 (>CH₂), 29.56 (>CH₂), 39.74 (>CH₂), 108.16, 108.36, 111.94, 115.59, 117.56, 118.07, 121.43, 136.13, 139.60, 149.14, 152.88, 156.97, 158.35, 160.26, 161.35 (>C=O); Anal. for C₁₉H₁₈FN₅O₂S (399.44): calcd.: C, 57.13; H, 4.54; N, 17.53; found: C, 57.26; H, 4.57; N, 17.80.

N'-(1-Butyl-5-chloro-2-oxoindolin-3-ylidene)-6-methylimidazo[2,1-*b*]thiazole-5-carbohydrazide (**6k**)

Yield = 67%; m.p. = 224–225 °C; IR: 1693 (>C=O), 3224 (>N-H); ¹H NMR: 0.85 (t, $J = 7.5$ Hz, 3H, -CH₃), 1.27–1.32 (m, 2H, >CH₂), 1.55–1.58 (m, 2H, >CH₂), 2.68 (s, 3H, -CH₃), 3.74 (t, $J = 7.5$ Hz, 2H, >CH₂), 7.24 (d, $J = 8.1$ Hz, 1H, Ar-H), 7.46–7.49 (m, 2H, Ar-Hs), 7.56 (s, 1H, Ar-H), 8.25 (d, $J = 4.0$ Hz, 1H, Ar-H), 13.19 (s, 1H, >N-H); ¹³C NMR: 14.02 (-CH₃), 15.99 (-CH₃), 20.00 (>CH₂), 30.56 (>CH₂), 40.52 (>CH₂), 43.69, 44.96, 118.70, 121.10, 122.18, 125.52, 126.31, 127.96, 130.24, 138.18, 144.56, 149.16, 157.09, 161.58 (>C=O); Anal. for C₁₉H₁₈ClN₅O₂S (415.90): calcd.: C, 54.87; H, 4.36; N, 16.84; found: C, 55.06; H, 4.38; N, 17.00.

N'-(5-Romo-1-butyl-2-oxoindolin-3-ylidene)-6-methylimidazo[2,1-*b*]thiazole-5-carbohydrazide (**6l**)

Yield = 39%; m.p. = 237–238 °C; IR: 1693 (>C=O), 3228 (>N-H); ¹H NMR: 0.86 (t, $J = 7.1$ Hz, 3H, -CH₃), 1.27–1.33 (m, 2H, >CH₂), 1.53–1.57 (m, 2H, >CH₂), 2.66 (s, 3H, -CH₃), 3.71 (t, $J = 7.5$ Hz, 2H, >CH₂), 7.16 (s, 1H, Ar-H), 7.44 (d, $J = 5.0$ Hz, 1H, Ar-H), 7.58 (s, $J = 9.5$ Hz, 1H, Ar-H), 7.63 (s, 1H, Ar-H), 8.22 (s, 1H, Ar-H), 13.14 (s, 1H, >N-H); ¹³C NMR: 14.00 (-CH₃), 16.99 (-CH₃), 20.00 (>CH₂), 29.56 (>CH₂), 40.52 (>CH₂), 40.69, 40.76, 112.72, 115.48, 115.61, 117.55, 121.78, 123.30, 134.13, 142.42, 149.18, 152.90, 156.93, 160.97 (>C=O); Anal. for C₁₉H₁₈BrN₅O₂S (460.35): calcd.: C, 49.57; H, 3.94; N, 15.21; found: C, 49.52; H, 4.08; N, 15.34.

3.1.3. Synthesis of Urea Derivatives **8a–g**

Compound **4** was stirred for 3 h in a solution of NaNO₂ with HCl to form the 6-methylimidazo[2,1-*b*]thiazole-5-carbonyl azide [**41**]. Azide **7** (0.21 g, 1 mmol) was refluxed in 1,4-dioxane (40 mL) with different anilines (1.0 mmol) for 8 h. Crystallization from EtOH for the formed solid gave the targeted urea derivatives **8a–g**, respectively.

1-(6-Methylimidazo[2,1-*b*]thiazol-5-yl)-3-phenylurea (**8a**)

Yield = 54%; m.p. = 287–288 °C; IR: 1639 (>C=O), 3263 (>N-H), 3290 (>N-H); ¹H NMR: 2.09 (s, 3H, -CH₃), 6.92 (t, $J = 7.5$ Hz, 1H, Ar-H), 7.08 (d, $J = 4.5$ Hz, 1H, Ar-H), 7.22 (t, $J = 7.4$ Hz, 1H, Ar-H), 7.42 (d, $J = 7.8$ Hz, 2H, Ar-Hs), 7.53 (d, $J = 5.0$ Hz, 1H, Ar-H), 8.09 (s, 1H, NH), 8.93 (s, 1H, >N-H); ¹³C NMR: 13.36 (-CH₃), 112.05, 118.63, 118.98 (3C), 122.48, 129.21 (2C), 137.23, 140.25, 144.81, 154.18 (>C=O); Anal. for C₁₃H₁₂N₄OS (272.33): calcd.: C, 57.34; H, 4.44; N, 20.57; found: C, 57.17; H, 4.26; N, 20.79.

1-(6-Methylimidazo[2,1-*b*]thiazol-5-yl)-3-(*p*-tolyl)urea (8b)

Yield = 47%; m.p. = 282–283 °C; IR: 1701 (>C=O), 3267 (>N-H), 3360 (>N-H); ¹H NMR: 2.14 (s, 3H, -CH₃), 2.25 (s, 3H, -CH₃), 7.08 (d, *J* = 8.0 Hz, 2H, Ar-Hs), 7.13 (d, *J* = 4.4 Hz, 1H, Ar-H), 7.36 (d, *J* = 7.8 Hz, 2H, Ar-Hs), 7.57 (d, *J* = 4.4 Hz, 1H, Ar-H), 8.09 (s, 1H, >N-H), 8.83 (s, 1H, >N-H); ¹³C NMR: 13.35 (-CH₃), 20.87 (-CH₃), 112.05, 118.70, 118.98, 119.13 (2C), 129.60 (2C), 131.32, 137.19, 137.65, 144.79, 154.20 (>C=O); Anal. for C₁₄H₁₄N₄OS (286.35): calcd.: C, 58.72; H, 4.93; N, 19.57; found: C, 58.66; H, 5.10; N, 19.59.

1-(4-Methoxyphenyl)-3-(6-methylimidazo[2,1-*b*]thiazol-5-yl)urea (8c)

Yield = 50%; m.p. = 284–285 °C; IR: 1639 (>C=O), 3140 (>N-H), 3278 (>N-H); ¹H NMR: 2.08 (s, 3H, -CH₃), 3.66 (s, 3H, -O-CH₃), 6.80 (d, *J* = 8.5 Hz, 2H, Ar-H), 7.08 (d, *J* = 4.5 Hz, 1H, Ar-H), 7.32 (d, *J* = 8.5 Hz, 2H, Ar-Hs), 7.52 (d, *J* = 5.0 Hz, 1H, Ar-H), 8.04 (s, 1H, >N-H), 8.74 (s, 1H, >N-H); ¹³C NMR: 13.37 (-CH₃), 55.67 (-O-CH₃), 111.98, 114.37 (2C), 118.83, 120.6 (2C), 133.29, 137.13, 144.73, 144.73, 154.37, 155.05 (>C=O); Anal. for C₁₄H₁₄N₄O₂S (302.35): calcd.: C, 55.62; H, 4.67; N, 18.53; found: C, 55.35; H, 4.69; N, 18.45.

1-(4-Fluorophenyl)-3-(6-methylimidazo[2,1-*b*]thiazol-5-yl)urea (8d)

Yield = 56%; m.p. = 281–282 °C; IR (KBr): 1635 (>C=O), 3163 (>N-H), 3278 (>N-H); ¹H NMR: 2.08 (s, 3H, -CH₃), 7.04–7.10 (m, 3H, Ar-Hs), 7.42–7.44 (m, 2H, Ar-Hs), 7.54 (d, *J* = 5.0 Hz, 1H, Ar-H), 8.12 (s, 1H, >N'-H), 8.98 (s, 1H, >N-H); ¹³C NMR: 13.36 (-CH₃), 112.07, 115.59 (2C), 115.76 (2C), 118.58, 118.98, 120.82, 136.62, 137.29, 144.84, 154.29 (>C=O); Anal. for C₁₃H₁₁FN₄OS (290.32): calcd.: C, 53.78; H, 3.82; N, 19.30; found: C, 53.80; H, 4.02; N, 19.53.

1-(4-Chlorophenyl)-3-(6-methylimidazo[2,1-*b*]thiazol-5-yl)urea (8e)

Yield = 48%; m.p. = 285–286 °C; IR: 1708 (>C=O), 3267 (>N-H), 3360 (>N-H); ¹H NMR: 2.08 (s, 3H, -CH₃), 7.09 (d, *J* = 4.0 Hz, 1H, Ar-H), 7.26 (d, *J* = 9.0 Hz, 2H, Ar-Hs), 7.45 (d, *J* = 8.5 Hz, 1H, Ar-H), 7.54 (d, *J* = 4.5 Hz, 1H, Ar-H), 8.19 (s, 1H, >N-H), 9.12 (s, 1H, >N-H); ¹³C NMR: 13.36 (-CH₃), 112.10, 118.46, 118.99, 120.56 (2C), 126.00, 129.03 (2C), 137.35, 139.32, 144.89, 154.13 (>C=O); Anal. for C₁₃H₁₁ClN₄OS (306.77): calcd.: C, 50.90; H, 3.61; N, 18.26; found: C, 50.73; H, 3.84; N, 18.39.

1-(4-Bromophenyl)-3-(6-methylimidazo[2,1-*b*]thiazol-5-yl)urea (8f)

Yield = 50%; m.p. = 288–289 °C; IR: 1709 (>C=O), 3263 (>N-H), 3360 (>N-H); ¹H NMR: 2.08 (s, 3H, -CH₃), 7.09 (d, *J* = 4.5 Hz, 1H, Ar-H), 7.37–7.42 (m, 4H, Ar-Hs), 7.55 (d, *J* = 4.5 Hz, 1H, Ar-H), 8.27 (s, 1H, >N-H), 9.20 (s, 1H, >N-H); ¹³C NMR: 13.37 (-CH₃), 112.09, 113.87, 118.48, 119.00, 120.96 (2C), 131.92 (2C), 137.30, 139.79, 144.87, 154.12 (>C=O); Anal. for C₁₃H₁₁BrN₄OS (351.22): calcd.: C, 44.46; H, 3.16; N, 15.95; found: C, 44.68; H, 3.28; N, 16.17.

4-(3-(6-Methylimidazo[2,1-*b*]thiazol-5-yl)ureido)benzenesulfonamide (8g)

Yield = 56%; m.p. = 283–284 °C; IR: 1708 (>C=O), 3120 (>N-H), 3275 (>N-H); ¹H NMR: 2.09 (s, 3H, -CH₃), 7.09 (d, *J* = 4.5 Hz, 1H, Ar-H), 7.17 (s, 2H, -NH₂), 7.58 (d, *J* = 9.0 Hz, 1H, Ar-H), 7.57 (t, *J* = 8.5 Hz, 3H, Ar-Hs), 7.68 (d, *J* = 8.5 Hz, 2H, Ar-Hs), 8.26 (s, 1H, >N-H), 9.35 (s, 1H, >N-H); ¹³C NMR: 13.37 (-CH₃), 112.18, 118.26, 118.32 (2C), 119.01, 127.21 (2C), 137.39, 137.55, 143.42, 144.98, 153.99 (>C=O); Anal. for C₁₃H₁₃N₅O₃S₂ (351.40): calcd.: C, 44.43; H, 3.73; N, 19.93; found: C, 44.25; H, 3.56; N, 20.11.

3.2. Anticancer Activity

3.2.1. MTT Assay

The developed compounds were evaluated in vitro using the MTT cell viability assay following the published techniques [42,43] (Supplementary Data, page 42).

3.2.2. VEGFR-2 Kinase Activity

This assay was performed using the methodology described below. (Supplementary Data, page 42) [44,45].

3.2.3. PCR Assay

The gene expression levels of apoptosis genes were evaluated in MCF-7 cells using the following approaches in the Supplementary Data, page 43.

3.2.4. Cell Cycle Analysis and Apoptosis

These were performed using the approach described in the Supplementary Data, page 44 [46].

3.3. Docking Protocol

Docking studies were performed using AutoDockVina 1.5.7 (Supplementary Data, page 44).

3.4. In Silico Predictive ADME Study

The ADME study was performed using the SWISSADME server [47] (Supplementary Data, page 45).

4. Conclusions

Three derivatives, **6b**, **6i** and **6j**, of isatin–imidazo[2,1-*b*]thiazole hybrids with a carbohydrazide function as a linker showed significant anti-cancerous activity using the MTT assay, with the most active candidates being submitted for further investigation to test their invitro VEGFR-2 inhibitory efficacy compared to Sorafenib as a reference drug. The potent candidate **6i** was then subjected to a PCR study to measure Bax, Bcl2, caspase 8, caspase 9 and cytochrome C to understand the potency of the most active candidate **6i** on malignant cells. Ultimately, for the full investigation regarding its activity, **6i** was utilized for the cell cycle and apoptosis. It additionally arrested the cell cycle in the G2/M phase and induced apoptosis at rates higher than a standard drug. A docking protocol and ADME study were also performed and our candidates had the same binding mode of Sorafenib through interactions with the amino acid residues Lys868, Cys1045, Glu885 and Asp1046. As a consequence, **6i** was specified as a promising lead for additional research to design efficient anti-cancer agents.

Supplementary Materials: The following supporting information can be downloaded at: <https://www.mdpi.com/article/10.3390/ph17020216/s1>, Figures S1 and S2 and Table S1 (Molecular docking); Figure S3 and Table S2 (Virtual ADME assessment); Figures S4–S19 (¹H NMR and ¹³C NMR spectra of **6a–l**); Figures S20–S33 (¹H NMR and ¹³C NMR spectra of **8a–g**).

Author Contributions: Conceptualization, methodology, software, validation, formal analysis, investigation, resources, data curation, writing—original draft preparation, M.K.E. and M.S.E.; writing—review and editing, visualization, M.K.E., M.S.E. and N.A.A.; supervision, H.A.A.-A.; project administration, N.A.A.; funding acquisition, N.A.A. All authors have read and agreed to the published version of the manuscript.

Funding: Princess Nourah bint Abdulrahman University Researchers Supporting Project number (PNURSP2024R403), Princess Nourah bint Abdulrahman University, Riyadh, Saudi Arabia.

Institutional Review Board Statement: Not applicable.

Informed Consent Statement: Not applicable.

Data Availability Statement: Data is contained within the article and supplementary material.

Conflicts of Interest: The authors declare no conflicts of interest.

References

1. Ferlay, J.; Soerjomataram, I.; Dikshit, R.; Eser, S.; Mathers, C.; Rebelo, M.; Parkin, D.M.; Forman, D.; Bray, F. Cancer incidence and mortality worldwide: Sources, methods and major patterns in GLOBOCAN 2012. *Int. J. Cancer* **2015**, *136*, E359–E386. [[CrossRef](#)] [[PubMed](#)]
2. Pincheira, J. Invited Review Cell proliferation and cancer. *Histol. Histopathol.* **1998**, *13*, 1197–1214.
3. Folkman, J. Angiogenesis: An organizing principle for drug discovery? *Nat. Rev. Drug Discov.* **2007**, *6*, 273–286. [[CrossRef](#)] [[PubMed](#)]
4. Karamysheva, A.F. Mechanisms of angiogenesis. *Biochemistry* **2008**, *73*, 751–762. [[CrossRef](#)] [[PubMed](#)]
5. Kerbel, R.S. Tumor angiogenesis: Past, present and the near future. *Carcinogenesis* **2000**, *21*, 505–515. [[CrossRef](#)] [[PubMed](#)]
6. Traxler, P. Tyrosine kinases as targets in cancer therapy—Successes and failures. *Expert Opin. Ther. Targets* **2003**, *7*, 215–234. [[CrossRef](#)] [[PubMed](#)]
7. Guo, S.; Colbert, L.S.; Fuller, M.; Zhang, Y.; Gonzalez-Perez, R.R. Vascular endothelial growth factor receptor-2 in breast cancer. *Biochim. Biophys. Acta Rev. Cancer* **2010**, *1806*, 108–121. [[CrossRef](#)] [[PubMed](#)]
8. Bando, H.; Weich, H.A.; Brokelmann, M.; Horiguchi, S.; Funata, N.; Ogawa, T.; Toi, M. Association between intratumoral free and total VEGF, soluble VEGFR-1, VEGFR-2 and prognosis in breast cancer. *Br. J. Cancer* **2005**, *92*, 553–561. [[CrossRef](#)]
9. Zhu, X.; Zhou, W. The emerging regulation of VEGFR-2 in triple-negative breast cancer. *Front. Endocrinol.* **2015**, *6*, 159. [[CrossRef](#)]
10. Shiau, J.P.; Wu, C.C.; Chang, S.J.; Pan, M.R.; Liu, W.; Ou-Yang, F.; Chen, F.M.; Hou, M.F.; Shih, S.L.; Luo, C.W. FAK regulates VEGFR2 expression and promotes angiogenesis in triple-negative breast cancer. *Biomedicines* **2021**, *9*, 1789. [[CrossRef](#)]
11. Holmes, K.; Roberts, O.L.; Thomas, A.M.; Cross, M.J. Vascular endothelial growth factor receptor-2: Structure, function, intracellular signalling and therapeutic inhibition. *Cell Signal* **2007**, *19*, 2003–2012. [[CrossRef](#)]
12. Narayanan, J.; Tamilanban, T.; Kumar, P.S.; Guru, A.; Muthupandian, S.; Kathiravan, M.K.; Arockiaraj, J. Role and mechanistic actions of protein kinase inhibitors as an effective drug target for cancer and COVID. *Arch. Microbiol.* **2023**, *205*, 238. [[CrossRef](#)]
13. Musumeci, F.; Radi, M.; Brullo, C.; Schenone, S. Vascular endothelial growth factor (VEGF) receptors: Drugs and new inhibitors. *J. Med. Chem.* **2012**, *55*, 10797–10822. [[CrossRef](#)]
14. El Hadi, S.R.A.; Lasheen, D.S.; Soliman, D.H.; Elrazaz, E.Z.; Abouzid, K.A.M. Scaffold hopping and redesign approaches for quinazoline based urea derivatives as potent VEGFR-2 inhibitors. *Bioorg. Chem.* **2020**, *101*, 103961. [[CrossRef](#)]
15. Fodor, D.; Jung, I.; Turdean, S.; Satala, C.; Gurzu, S. Angiogenesis of hepatocellular carcinoma: An immunohistochemistry study. *World J. Hepatol.* **2019**, *11*, 294–304. [[CrossRef](#)] [[PubMed](#)]
16. Peng, F.W.; Liu, D.K.; Zhang, Q.W.; Xu, Y.G.; Shi, L. VEGFR-2 inhibitors and the therapeutic applications thereof: A patent review (2012–2016). *Expert Opin. Ther. Pat.* **2017**, *27*, 987–1004. [[CrossRef](#)] [[PubMed](#)]
17. Oguro, Y.; Miyamoto, N.; Okada, K.; Takagi, T.; Iwata, H.; Awazu, Y.; Miki, H.; Hori, A.; Kamiyama, K.; Imamura, S. Design, synthesis, and evaluation of 5-methyl-4-phenoxy-5H-pyrrolo[3,2-d] pyrimidine derivatives: Novel VEGFR2 kinase inhibitors binding to inactive kinase conformation. *Bioorg. Med. Chem.* **2010**, *18*, 7260–7273. [[CrossRef](#)] [[PubMed](#)]
18. Aziz, M.A.; Serya, R.A.T.; Lasheen, D.S.; Abdel-Aziz, A.K.; Esmat, A.; Mansour, A.M.; Singab, A.N.; Abouzid, K. Discovery of Potent VEGFR-2 Inhibitors based on Furopyrimidine and Thienopyrimidine Scaffolds as Cancer Targeting Agents. *Sci. Rep.* **2016**, *6*, 24460. [[CrossRef](#)]
19. Dweedat, H.E.; Mahrous, H.; Ibrahim, H.S.; Abdel-Aziz, H.A. Analogue-based design, synthesis and biological evaluation of 3-substituted-(methylenediazono)indolin-2-ones as anticancer agents. *Eur. J. Med. Chem.* **2014**, *78*, 275–280. [[CrossRef](#)]
20. Eldehna, W.M.; Altoukhy, A.; Mahrous, H.; Abdel-Aziz, H.A. Design, synthesis and QSAR study of certain isatin-pyridine hybrids as potential anti-proliferative agents. *Eur. J. Med. Chem.* **2015**, *90*, 684–694. [[CrossRef](#)]
21. Fares, M.; Eldehna, W.M.; Abou-Seri, S.M.; Abdel-Aziz, H.A.; Aly, M.H.; Tolba, M.F. Design, synthesis and in Vitro antiproliferative activity of novel isatin-quinazoline hybrids. *Arch. Pharm.* **2015**, *348*, 144–154. [[CrossRef](#)]
22. Kamal, A.; Dastagiri, D.; Ramaiah, M.J.; Reddy, J.S.; Bharathi, E.V.; Srinivas, C.; Pushpavalli, S.N.; Pal, D.; Pal-Bhadra, M. Synthesis of imidazothiazole-chalcone derivatives as anticancer and apoptosis inducing agents. *ChemMedChem* **2010**, *5*, 1937–1947. [[CrossRef](#)]
23. Elsayi, A.E.; Elbadawi, M.M.; Nocentini, A.; Almahli, H.; Giovannuzzi, S.; Shaldam, M.; Salem, R.; Ibrahim, T.M.; Abdel-Aziz, H.A.; Supuran, C.T.; et al. 1,5-diaryl-1,2,4-triazole ureas as new SLC-0111 analogues endowed with dual carbonic anhydrase and VEGFR-2 inhibitory activities. *J. Med. Chem.* **2023**, *66*, 10. [[CrossRef](#)]
24. Fakhry, M.M.; Mattar, A.A.; Alsulaimany, M.; Al-Olayan, E.M.; Al-Rashood, S.T.; Abdel-Aziz, H.A. New Thiazolyl-Pyrazoline Derivatives as Potential Dual EGFR/HER2 Inhibitors: Design, Synthesis, Anticancer Activity Evaluation and In Silico Study. *Molecules* **2023**, *28*, 7455. [[CrossRef](#)]
25. Abdelsalam, E.A.; Abd El-Hafeez, A.A.; Eldehna, W.M.; El Hassab, M.A.; Marzouk, H.M.M.; Elaasser, M.M.; Abou Taleb, N.A.; Amin, K.M.; Abdel-Aziz, H.A.; Ghosh, P.; et al. Discovery of novel thiazolyl-pyrazolines as dual EGFR and VEGFR-2 inhibitors endowed with in vitro antitumor activity towards non-small lung cancer. *J. Enzyme Inhib. Med. Chem.* **2022**, *37*, 2265–2282. [[CrossRef](#)] [[PubMed](#)]
26. Elewa, M.A.F.; Eldehna, W.M.; Hamdan, A.M.E.; Abd El-kawi, S.H.; El-Kalaawy, A.M.; Majrashi, T.A.; Barghash, R.F.; Abdel-Aziz, H.A.; Hashem, K.S.; Al-Gayyar, M.M.H. WRH-2412 alleviates the progression of hepatocellular carcinoma through regulation of TGF- β / β -catenin/ α -SMA pathway. *J. Enzyme Inhib. Med. Chem.* **2023**, *38*, 2185761. [[CrossRef](#)] [[PubMed](#)]

27. Eldehna, W.M.; Mohammed, E.E.; Al-Ansary, G.H.; Berrino, E.; Elbadawi, M.M.; Ibrahim, T.M.; Jaballah, M.Y.; Al-Rashood, S.T.; Binjubair, F.A.; Celik, M.; et al. Design and synthesis of 6-arylpyridine-tethered sulfonamides as novel selective inhibitors of carbonic anhydrase IX with promising antitumor features toward the human colorectal cancer. *Eur. J. Med. Chem.* **2023**, *258*, 115538. [[CrossRef](#)]
28. El-Atawy, M.A.; Alshaye, N.A.; Elrubi, N.; Hamed, E.A.; Omar, A.Z. Pyrimidines-Based Heterocyclic Compounds: Synthesis, Cytotoxicity Evaluation and Molecular Docking. *Molecules* **2022**, *27*, 4912. [[CrossRef](#)] [[PubMed](#)]
29. Dietrich, J.; Hulme, C.; Hurley, L.H. The design, synthesis, and evaluation of 8 hybrid DFG-out allosteric kinase inhibitors: A structural analysis of the binding interactions of Gleevec[®], Nexavar[®], and BIRB-796. *Bioorg. Med. Chem.* **2010**, *18*, 5738–5748. [[CrossRef](#)]
30. Xie, Q.Q.; Xie, H.Z.; Ren, J.X.; Li, L.L.; Yang, S.Y. Pharmacophore modeling studies of type I and type II kinase inhibitors of Tie2. *J. Mol. Graph. Model.* **2009**, *27*, 751–758. [[CrossRef](#)]
31. Sobhy, M.K.; Mowafy, S.; Lasheen, D.S.; Farag, N.A.; Abouzid, K.A.M. 3D-QSAR pharmacophore modelling, virtual screening and docking studies for lead discovery of a novel scaffold for VEGFR 2 inhibitors: Design, synthesis and biological evaluation. *Bioorg. Chem.* **2019**, *89*, 102988. [[CrossRef](#)]
32. Abdel-Mohsen, H.T.; Abdullaziz, M.A.; El Kerdawy, A.M.; Ragab, F.A.F.; Flanagan, K.J.; Mahmoud, A.E.E.; Ali, M.M.; Diwani, H.I.E.; Senge, M.O. Targeting receptor tyrosine kinase VEGFR-2 in hepatocellular cancer: Rational design, synthesis and biological evaluation of 1,2-disubstituted benzimidazoles. *Molecules* **2020**, *25*, 770. [[CrossRef](#)] [[PubMed](#)]
33. Hyde, C.A.C.; Giese, A.; Stutfeld, E.; Abram Saliba, J.; Villemagne, D.; Schleier, T.; Binz, H.K.; Ballmer-Hofer, K. Targeting Extracellular Domains D4 and D7 of Vascular Endothelial Growth Factor Receptor 2 Reveals Allosteric Receptor Regulatory Sites. *Mol. Cell Biol.* **2012**, *32*, 3802–3813. [[CrossRef](#)] [[PubMed](#)]
34. Modi, S.J.; Kulkarni, V.M. Exploration of structural requirements for the inhibition of VEGFR-2 tyrosine kinase: Binding site analysis of type II, 'DFG-out' inhibitors. *J. Biomol. Struct. Dyn.* **2022**, *40*, 5712–5727. [[CrossRef](#)] [[PubMed](#)]
35. El-Adl, K.; Ibrahim, M.K.; Khedr, F.; Abulkhair, H.S.; Eissa, I.H. Design, synthesis, docking, and anticancer evaluations of phthalazines as VEGFR-2 inhibitors. *Arch. Pharm.* **2022**, *355*, e2100278. [[CrossRef](#)] [[PubMed](#)]
36. Liu, S.; Lin, Y.C. Transformation of MCF-10A human breast epithelial cells by zeranol and estradiol-17 β . *Breast J.* **2004**, *10*, 514–521. [[CrossRef](#)] [[PubMed](#)]
37. Li, J.; Fu, A.; Zhang, L. An Overview of Scoring Functions Used for Protein–Ligand Interactions in Molecular Docking. *Interdiscip. Sci.* **2019**, *11*, 320–328. [[CrossRef](#)]
38. Lipinski, C.A.; Dominy, B.W.; Feeney, P.J. Experimental and computational approaches to estimate solubility and permeability in drug discovery and development settings. *Adv. Drug Deliv. Rev.* **2001**, *46*, 3–26. [[CrossRef](#)] [[PubMed](#)]
39. Duchowicz, P.R.; Talevi, A.; Bellera, C.; Bruno-Blanch, L.E.; Castro, E.A. Application of descriptors based on Lipinski's rules in the QSPR study of aqueous solubilities. *Bioorg. Med. Chem.* **2007**, *15*, 3711–3719. [[CrossRef](#)]
40. Samala, G.; Devi, P.B.; Saxena, S.; Meda, N.; Yogeewari, P.; Sriram, D. Design, synthesis and biological evaluation of imidazo[2,1-b]thiazole and benzo[d]imidazo[2,1-b]thiazole derivatives as Mycobacterium tuberculosis pantothenate synthetase inhibitors. *Bioorganic Med. Chem.* **2016**, *24*, 1298–1307. [[CrossRef](#)]
41. Cesur, N.; Cesur, Z.; Guner, H. Fused Heterocycles: Synthesis of Some New Imidazothiazoles. *Heterocycl. Commun.* **2002**, *8*, 433–438. [[CrossRef](#)]
42. Slater, T.F.; Sawyer, B.; Sträuli, U.; van de Loosdrecht, A.A.; Beelen, R.H.J.; Ossenkoppele, G.J. Studies on succinate-tetrazolium reductase systems. III. Points of coupling of four different tetrazolium salts III. Points of coupling of four different tetrazolium salts. *J. Immunol. Methods* **1994**, *77*, 311–320.
43. van de Loosdrecht, A.A.; Beelen, R.H.J.; Ossenkoppele, G.J.; Broekhoven, M.G.; Langenhuijsen, M.M.A.C. A tetrazolium-based colorimetric MTT assay to quantitate human monocyte mediated cytotoxicity against leukemic cells from cell lines and patients with acute myeloid leukemia. *J. Immunol. Methods* **1994**, *174*, 311–320. [[CrossRef](#)] [[PubMed](#)]
44. Fontanella, C.; Ongaro, E.; Bolzonello, S.; Guardascione, M.; Fasola, G.; Aprile, G. Clinical advances in the development of novel VEGFR2 inhibitors. *Ann. Transl. Med.* **2014**, *2*, 123. [[PubMed](#)]
45. Sharma, K.; Suresh, P.S.; Mullangi, R.; Srinivas, N.R. Quantitation of VEGFR2 (vascular endothelial growth factor receptor) inhibitors—Review of assay methodologies and perspectives. *Biomed. Chromatogr.* **2015**, *29*, 803–834. [[CrossRef](#)] [[PubMed](#)]
46. Darzynkiewicz, Z. Critical aspects in analysis of cellular DNA content. *Curr. Protoc. Cytom.* **2011**, *7*, 7.2.1–7.2.8. [[CrossRef](#)]
47. Daina, A.; Michielin, O.; Zoete, V. SwissADME: A free web tool to evaluate pharmacokinetics, drug-likeness and medicinal chemistry friendliness of small molecules. *Sci. Rep.* **2017**, *7*, 42717. [[CrossRef](#)]

Disclaimer/Publisher's Note: The statements, opinions and data contained in all publications are solely those of the individual author(s) and contributor(s) and not of MDPI and/or the editor(s). MDPI and/or the editor(s) disclaim responsibility for any injury to people or property resulting from any ideas, methods, instructions or products referred to in the content.